





# In situ resistivity measurement of metal surfaces to track down dislocations caused by high field conditioning

M. Coman<sup>1</sup> , M. Jacewicz<sup>1</sup> and D. Dancila<sup>1,2</sup> 

<sup>1</sup>FREIA, Department of Physics and Astronomy, Uppsala University, Uppsala, Sweden and <sup>2</sup>Microwave Group, Department of Electrical Engineering, Uppsala University, Uppsala, Sweden

## Research Paper

**Cite this article:** Coman M, Jacewicz M, Dancila D (2023). In situ resistivity measurement of metal surfaces to track down dislocations caused by high field conditioning. *International Journal of Microwave and Wireless Technologies* 1–9. <https://doi.org/10.1017/S1759078723001411>

Received: 22 June 2023  
Revised: 20 November 2023  
Accepted: 21 November 2023

**Keywords:**  
dislocations; high gradient conditioning; quality factor; resistivity measurement

**Corresponding author:** M. Coman;  
Email: [mircea.coman@physics.uu.se](mailto:mircea.coman@physics.uu.se)

### Abstract

Conditioning of a metal surface in a high-voltage system is the progressive development of resistance to vacuum arcing over the operational life of the system. This is relevant for accelerator cavities, where high level of performance is only achievable after a long conditioning period. Beyond the accelerator research field, this is an important topic for any technology where breakdowns can cause device failure, either by directly disrupting device operation or by causing cumulative hardware damage.

We are developing a direct method to measure the surface resistivity of a metal surface that is being conditioned with a HV DC system by inducing a high frequency (GHz) radio-frequency current in the parallel-plate electrode system. If the system can function as a resonant cavity, the surface resistivity data would be encoded in its quality factor (*Q*-factor). The changes in the resistivity measured in cryogenic conditions would indicate a formation of dislocations under the surface, something that has been speculated as an important process behind the conditioning.

In this paper, we present two modified designs of the electrode system, which will act as a resonant cavity, the results of 3D EM simulations and experimental results regarding the characterization of this resonant system.

## Introduction

High electrical fields in ultra-high vacuum environments (UHV) are needed in many areas of research and for many technologies, such as high energy accelerators, high vacuum interrupters, fusion research, electron and X-ray sources, and many others [1, 2]. In particular, in particle accelerators, high electrical fields are needed to accelerate particles to high energies. The performance of accelerating cavities is limited by the electrical discharges that can take place even in ultra-high vacuum environments, called vacuum arc breakdowns. In this situation, the conductive plasma that forms the electrical discharges is composed of metal vapors and electrons from the metal surface of the cavity.

Vacuum arc breakdowns are already observed at applied fields less than 100 MV m<sup>-1</sup>. But these fields are 100 times smaller than the fields that are needed for the start of the breakdown reaction (~10.8 GV m<sup>-1</sup>) [3]. The most common explanation for this discrepancy is that there are sharp nano-protrusion on the metal surface which amplify the field by approximately 100 times. The breakdown reaction always starts with the field emission of electrons from the negatively charged electrode (the cathode) [4–7]. This fact plays an important role in the design of our resonant system because sharp corners on the surface of the cathode need to be avoided. Otherwise, because of the field enhancement at these corners, most breakdowns will form in these areas.

It has been observed that when high electrical field pulses are applied to the surface repeatedly, the accepted electrical field (the field at which there are almost no breakdowns) increases [8, 9]. This process is called conditioning. A traditional explanation for the conditioning process is that the sharp features on the electrode surface are destroyed during the breakdowns, and so higher fields can be applied to the surface without further breakdowns. But experimental data shows that this is not a complete explanation. Firstly, when the electrodes are unconditioned, their surface is very smooth, with a mirror-like finish. But, after conditioning, because of the breakdown craters, the surface is much rougher. Even if the surface is rougher after conditioning, it can sustain a higher electrical field than the smooth, polished surface of the unconditioned electrodes. Moreover, in [8, 10], it has been shown that the maximum field that is accepted by a metal surface correlates well with the crystal structure of the metal. Furthermore, in [9], it has been shown that the conditioning effect correlates to the number of applied pulses,

© The Author(s), 2023. Published by Cambridge University Press in association with the European Microwave Association. This is an Open Access article, distributed under the terms of the Creative Commons Attribution licence (<http://creativecommons.org/licenses/by/4.0>), which permits unrestricted re-use, distribution and reproduction, provided the original article is properly cited.

and not with the number of breakdowns, suggesting that the conditioning is done by the electric field pulses, and not by the breakdowns.

The truth seems therefore more complicated, and the modern understanding is that there are extrinsic and intrinsic mechanisms responsible for the breakdown generation [4, 11, 12]. The external factors are aforementioned irregularities or contamination of the electrode surface. The second mechanism is related to the material properties and alters the breakdown rate even when the effect of extrinsic processes was exhausted by cleaning of the surface via initial “cleaning” by plasma from discharges. The research into the mechanisms behind intrinsic breakdown generation is an active field of study for the last decade and currently theoretical models hint on a possibility for the formation of protrusions on a metallic surface that is held at a sufficiently high electric field in the presence of a near-surface crystallographic defects. Our understanding of the dislocation and void nucleation processes occurring in the strained metals is advancing, but not yet complete. In recent years, theoretical models and simulations were presented supporting the hypothesis of intrinsic process connected with the changes under surface [13, 14]. These are thermally activated processes, initiated by electron field emission, accompanying the plastic deformation caused by tensile stress due to an applied electric field [15, 16].

One hypothesis explains the breakdown nucleation as emanation of sharp features from the surface due to plastic activity of the collective dislocations within the surface layer of samples exposed to high electric fields [17].

One can routinely observe with microscopy methods extensive mobile dislocation structures in the soft, large-grained OFHC copper. However, due to experimental difficulties, we are missing a clear characteristic that these structures are modified due to exposure to high fields [18, 19], and we are only left with hints. For instance, the model predicts that the movement of dislocations would be accompanied by characteristic pre-breakdown fluctuations to be observed as spikes in the field emissions between the electrodes. Recently such fluctuations has been measured with the rate in agreement with the predictions of the dislocation model [20, 21].

A side effect of the change in the dislocation density is that the resistivity of the metal increases [22]. In this paper, we are presenting the basis for a system that can measure in-situ the changes in the surface resistivity of metal electrodes exposed to extreme fields, in order to obtain information about the creation of dislocations underneath their surface.

## Method

Direct measurements regarding the formation and movement of the dislocations during conditioning was not attempted previously to our knowledge. Indirect observation via microscopic methods on the other hand is not conclusive. Therefore, a new characterization method, one that could be used during the conditioning, has been sought after. One important parameter of the surface clearly linked with the presence of the crystallographic defects, such as dislocations, and which could be monitored, is its electric resistivity.

### Surface resistivity changes at cryogenic temperatures

In general, the resistivity of a metal,  $\rho_{total}$  can be decomposed in three terms, which correspond to the electron-phonon scattering ( $\rho_{phonons}$ ), the electron-impurities scattering ( $\rho_{impurities}$ ) and the

electron-defects scattering ( $\rho_{defects}$ ):

$$\rho_{total}(T) = \rho_{phonons}(T) + \rho_{impurities} + \rho_{defects}, \quad (1)$$

where  $\rho_{phonons}$  can be described by Block-Grüneisen formula [23] with Debye's temperature,  $\Theta_D$ :

$$\rho_{phonons}(T) \propto \left(\frac{T}{\Theta_D}\right)^5 \int_0^{\Theta_D/T} \frac{t^5}{(e^t - 1)(1 - e^{-t})} dt. \quad (2)$$

The electron-phonon term is linear at high temperature, and it transforms smoothly into a  $T^5$  dependence at low temperature, becoming negligible with respect to other terms, which are constant with respect to the temperature. Therefore, investigating resistivity changes at ultra-low temperatures is advantageous because in cryogenic conditions, the resistivity is related only to the scattering of the electrons off the impurities and off lattice defects (such as dislocations), and not by the interaction between electrons and phonons.

Experiments made by mechanically deforming very pure copper samples show that the dislocation specific resistivity (DSR), defined as the ratio between the resistivity due to dislocations ( $\rho_D$ ) and the density of dislocations ( $n_D$ ) is constant for samples with a dislocation density greater than  $10^9 \text{ cm}^{-2}$  [24]:

$$DSR = \frac{\rho_D}{n_D} = (1.6 \pm 0.2) \times 10^{-19} \Omega \text{ cm}^3. \quad (3)$$

So far, there is no data regarding the expected increase in dislocation density that we should expect during conditioning. Some cross-sections of conditioned surfaces were observed under TEM in order to try to quantify the effects of conditioning on dislocation density [18]. But unfortunately, the observations made so far are not conclusive [19].

### Sensitivity to thin, subsurface layer

According to the simulations, the stress due to high field affects the crystallographic defects only near the surface of the electrodes, a few hundred nanometers deep [11].

It is, therefore, important to measure the change in resistivity only in the volume close to the surface. For this reason, the use of microwave resonant cavity method to obtain data about the resistivity near the metal surface seems ideal. The electromagnetic fields that oscillate in time with a given frequency,  $\omega$ , cannot penetrate the bulk volume of a good conductor. Instead, they will be exponentially attenuated near the surface. The amplitude of the fields will decay by an amount equal to  $1/e \approx 36.8\%$  after traveling a distance equal to one skin depth,  $\delta$  defined as [25]:

$$\delta = \sqrt{\frac{2\rho}{\omega\mu}}, \quad (4)$$

where  $\rho$  is the resistivity and  $\mu$  is the magnetic permeability of the conductor. The current induced in the metal, and therefore the ohmic losses, will also be localized near the surface a few skin depths deep.

It is important to note that the skin depth is inversely proportional to the square root of the frequency. If we were to use a direct current method of measuring the resistivity, such as a 4-point probe,  $\omega \rightarrow 0$  and  $\delta \rightarrow \infty$ . This means that the current penetrates in the bulk of the material and that the measured resistivity will correspond to the resistivity measured in the bulk. On the other hand, for a frequency of around 4 GHz,  $\delta = 1 \mu\text{m}$  at room temperature (RT) and  $\delta = 100 \text{ nm}$  at cryogenic temperatures, where we expected the resistivity to decrease by 100 times.

But in cryogenic conditions, the calculations for the field attenuation below the metal surface are more complicated. While the free mean path ( $l$ ) in copper is inversely proportional to its resistivity ( $\rho l = 6.6 \times 10^{-16} \Omega \text{m}^2$  [26]), the skin depth is proportional to the square root of the resistivity. As the copper electrodes are cooled down and their resistivity decreases, the skin depth decreases and the mean free path increases. At 4K, the mean free path ( $l = 4.2 \mu\text{m}$ ) will be an order of magnitude larger than the skin depth. In these conditions, most conduction band electrons will travel deeper than a few skin depths without suffering any collisions. This will give rise to a current and to electromagnetic fields much deeper than a few skin depths, down to depths on the order of the mean free path, which does not depend on the frequency. The electromagnetic fields do not decrease exponentially, so the concept of skin depth is not well defined in this case. But it can be calculated that the magnitude of the electric field drops by 90% of its value at the surface at a depth equal to  $l/4 \approx 1 \mu\text{m}$ . This effect is called in the literature the anomalous skin effect [27].

Therefore, the measured resistivity will allow us to obtain information exclusively about the defects that are less than a micron underneath the surface. A limitation of this method is that as we condition, the resistivity is expected to increase and the mean free path to decrease, which means that we sample different depths, depending on the change in resistivity.

### Experimental setup for cold surface conditioning

The proposed method is of general use, but in the following chapters we suggest possible adaptations of an existing cryogenic high-voltage direct-current (DC) system based on a stand-alone cryocooler at the Freia Laboratory in Uppsala, Sweden [28].

The setup consists of two parallel-plate metal electrodes, with a radius of 31 mm, separated by an alumina ( $\text{Al}_2\text{O}_3$ ) spacer, as shown in Fig. 1. The spacer is manufactured precisely such that the gap between the electrodes is approximately  $40 \mu\text{m}$  at RT and  $60 \mu\text{m}$  at cryogenic temperatures. The electrodes are placed in ultra-high vacuum, inside a cryostat, where variable temperatures, down to 4K, can be reached. The conditioning is done using high voltage DC pulses (0.5–10 kV), and thus achieving fields of the order of ( $100\text{--}200 \text{ MVm}^{-1}$ ) with a repetition rate of up to 1 kHz [28]. The high voltage DC pulses are generated by a solid-state Marx generator with 15 stages that was designed for this type of conditioning experiments [29].

We aim to use this cryogenic DC system for electrode conditioning and to extend the experimental set-up with an additional vector network analyzer (VNA) to induce a high frequency (GHz) current in between the electrodes. In order to be able to make RF resistivity measurements, the electrode assembly needs to be modified such that a resonant mode can be excited and contained in between the electrodes. A schematic of this set-up is shown in Fig. 1. The VNA and the HV generator will not be connected at the same time, but they will be connected and disconnected manually when needed.

### Measurement method

Information about the relative changes in resistivity less than a micrometer below the metal surface can be extracted from the quality factor of the resonant mode of the modified electrode system. The quality factor can be obtained from reflection-type or transmission-type measurements. The former one is chosen in

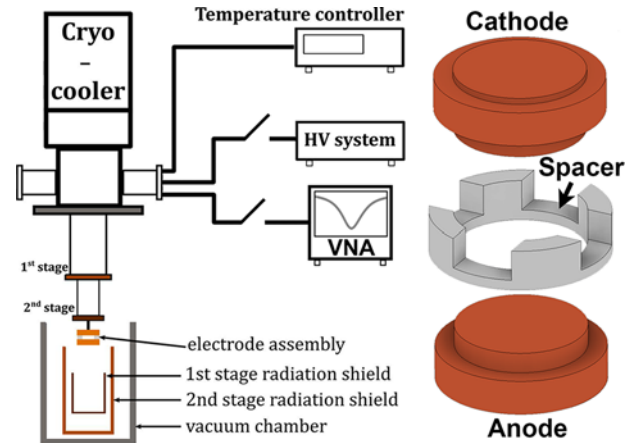


**Figure 1.** Left: The experimental set-up with the VNA added. The switches between the HV generator and the VNA represent physical connections that will be connected and disconnected manually. Right: A closer look at the electrode assembly.

favor of the latter in order to minimize the added thermal load of an additional cable inside the cryostat.

In between cycles of pulses done by the DC generator, the DC generator is disconnected and a VNA will be connected. In the first series of the experiments, we plan to disconnect and connect the DC generator and the VNA manually. The VNA will measure the complex reflection coefficients near the resonant frequency of the system. Ideally, these coefficients, plotted on the complex plane, will form a perfect circle, called the Q-circle [30]. The Q-circle is then fitted using the algorithm described by Kajfez in [31, 32], and the more general algorithms, which can account for phase delay in uncalibrated transmission lines, such as the QFIT7 algorithm, described in [30].

The relation between the quality factor and the surface resistivity ( $R_s$ ) is:

$$Q_0 = \frac{G}{R_s}, \quad (5)$$

where  $G$  is a geometric factor that depends only on the geometry of the resonant system and on the resonant mode that is being used. At RT, when the mean free path of the electrons is much smaller than the skin depth, the surface resistivity can be calculated as:

$$R_s = \frac{\rho}{\delta} = \sqrt{\frac{\omega \mu \rho}{2}}. \quad (6)$$

But in cryogenic temperatures, when the mean free path is an order of magnitude larger than the skin depth, the field “seen” by a conduction band electron between successive collisions cannot be considered to be constant and the measured surface resistivity will be larger than the one calculated from eq. 6. Using the Mathematica notebook from [33], which implemented the equations from [27], the surface resistivity ( $R_s$ ) can be calculated from resistivity ( $\rho$ ) in this anomalous regime. In Fig. 2, the relative change in  $R_s$  is shown as a function of relative change in  $\rho$ , for a copper sample with  $\rho_{293K} / \rho_{4K} = 100$  for the two frequencies used in this paper.

In these experiments, we are only interested in measuring the relative changes in dislocation density, rather than the absolute value of the dislocation density itself. The latter is also quite difficult to measure because of the complicated geometry of the system and because of the uncertainty in measuring precisely the gap size

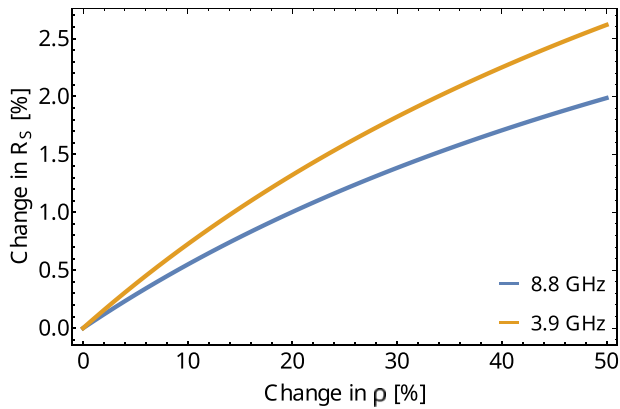


**Figure 2.** The relative change in surface resistivity ( $R_s$ ), and thus of  $Q_0$ , as a function of the relative change in resistivity ( $\rho$ ).

after cooling down to cryogenic temperatures. As a result of these uncertainties in extraction of the geometrical factor, it can be problematic to obtain an exact value for the surface resistivity from the quality factor. Instead, we plan to measure only the relative change in quality factor, which will provide information about the relative change in resistivity and thus about the relative change in dislocation density underneath the surface.

Previously [32], we have measured quality factor changes of around 0.3%, induced by varying the temperature of some test cavities. Applying the same methods to our current case, these small changes in quality factor, and thus in surface resistivity, would translate to a 4% change in the bulk resistivity very close to the surface.

### Novel designs for resistivity measurements

In order to contain a resonant mode in the gap between the electrodes, the electrode surface should be modified. Because the breakdowns are initiated from the cathode, leading with field emission, it is important to avoid sharp features on the surface of the cathode, which would enhance the electrical field, resulting in non-uniform field distribution and breakdown damage at these locations. Therefore, all modifications should be made only on the anode surface in order to avoid field enhancement effects. Moreover, in the future, for experiments which involve metals or alloys that are difficult to machine, the cathode can be made out of the desired material, while keeping the anode made out of copper, which can be machined easily.

Two designs have been proposed, both sharing a feature inspired by Shintake's choke mode cavity design [34]. The main modification comes in a form of a circular groove with a height equal to a quarter of the wavelength of the resonant mode that would be machined in the surface of the electrode a few mm away from its edge, like in Fig. 3. This groove, called the choke, can be modeled as a perfect magnetic wall and electromagnetic modes can be excited in the area delimited by the groove. The resonant modes of such a cavity are those of a parallel plate resonator. The frequencies of such a cavity can be calculated analytically [35]:

$$f_{TM_{nm0}} = \frac{c_0 \gamma_{nm}}{2\pi r}, \quad (7)$$

where  $c_0 = 3 \times 10^8$  is the speed of light in vacuum,  $\gamma_{nm}$  are the roots of the Bessel functions  $J'_n(\gamma_{nm}) = 0$  and  $r$  is the radius of

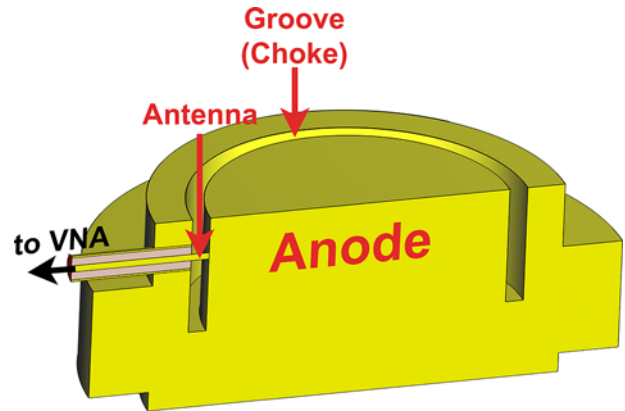


**Figure 3.** A cross-section through the anode and through the antenna.

the cavity. In the case of our choke cavity,  $r$  is the inner radius of the groove.

The main difference between the two designs comes from the way in which the RF signal is introduced between the plates. In the following, copper was selected for the material of the electrodes and used in the simulations and the experiments.

### First design

In the first design, we aim to modify only the anode. In order to contain the resonant mode between the electrode, a circular groove (the choke) is machined in the surface of the anode. The thickness of the choke is chosen to be 2.7 mm and its inner radius is chosen to be 22.65 mm. Using eq. 7, we find that the fundamental mode of this structure,  $TM_{110}$ , has a frequency equal to 3.9 GHz. Therefore, the height of the choke should be equal to 19 mm. This modified design of the anode is shown in Fig. 3.

To couple to the fundamental mode, shown in Fig. 4(a), we introduce an antenna through a hole in the side of the anode. The tip of the antenna is in contact with the inner wall of the choke, as shown in Fig. 3, forming a loop. Unfortunately, this method of coupling can also excite resonant modes outside the area delimited by the choke, very close in frequency to the fundamental mode, like the one in Fig. 4(b). This additional parasitic resonance can add uncertainties when the Q-circle is fitted in order to obtain the quality factor of the fundamental mode.

To get rid of this mode, we need to cut current lines by machining notches in the areas where the magnetic field (and therefore

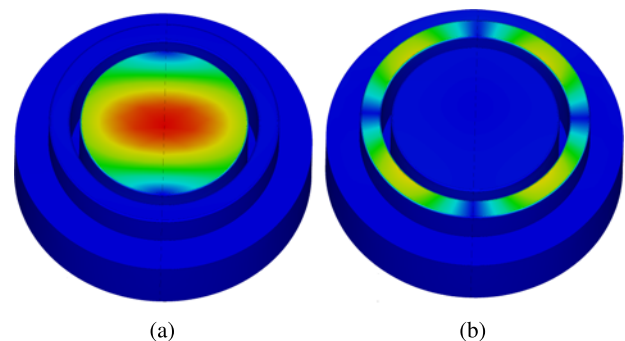


**Figure 4.** The magnetic field distributions of the fundamental (a) and of the parasitic mode (b).

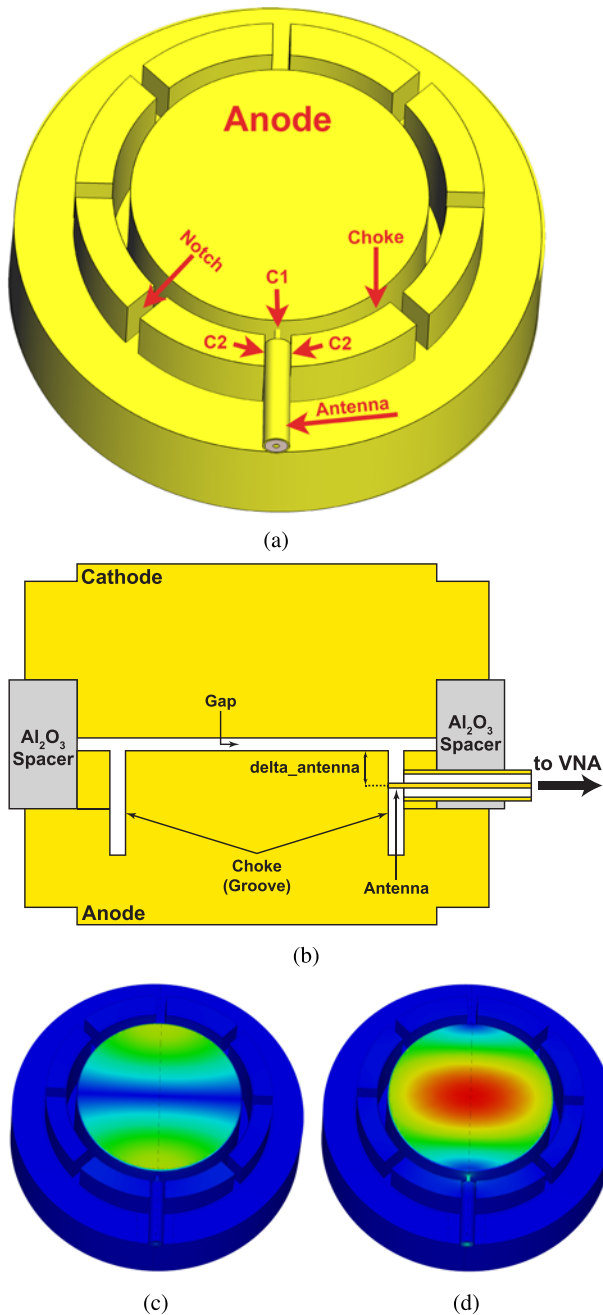


**Figure 5.** 3D model of the modified cathode in the first design (points labeled C2 and C1 represent the points at which good electrical contact is needed) (a), the schematic showing a vertical section through the modified electrode system (not to scale) (b), and the electric (c) and the magnetic (d) field distributions for the fundamental mode of the system,  $TM_{110}$ .

the current) have a maximum. Eight such notches are machined, even though the mode shown in Fig. 4(b) has four maxima. This is done in order to account for both linearly independent orientations of the parasitic mode. The thickness of these notches is 2.7 mm, with the exception of one notch, which has a thickness of 4 mm. The thicker notch will be used to introduce the antenna in the choke, as shown in Fig. 5(a). A cross-section through both electrodes and the antenna is shown in Fig. 5(b).

The electromagnetic field distributions for the fundamental mode of this design are shown in Fig. 5(c) and (d). The frequency

obtained from simulations is equal to the analytically calculated value, 3.9 GHz. The area most sensitive to changes in resistivity is the area where the magnetic field is maximum. Therefore, our measurements will be more sensitive to changes in dislocation density in the center of the electrodes.

The quality factor of the fundamental mode of this cavity, obtained from CST Studio [36] simulations, is  $Q_0 = 39$  at RT (with a gap size of  $40 \mu\text{m}$ ) and  $Q_0 = 580$  at cryogenic temperatures (with a gap size of  $60 \mu\text{m}$ ), where we expect the bulk resistivity to decrease by a factor of 100. For a gap size equal to  $75 \mu\text{m}$ , as it was used during the experimental testing of this design, the quality factor obtained from simulations is equal to 74.

The electrical contact between the tip of the antenna and the inner wall of the choke (the point label C1 in Fig. 5(a)), as well as the contact between the copper shield of the antenna and the side walls of the notches (C2 in Fig. 5(a)) are crucial. For this reason, it is important to make sure that these contacts are maintained as the electrodes and connectors shrink due to thermal contraction when cooling down. The second design, described in the next section, does not have this problem.

We have also made simulations in which a second antenna is added in order to make transmission measurements. The antennas were placed  $90^\circ$  and  $180^\circ$  apart. When the antennas are  $90^\circ$  apart, there is little transmission (Fig. 6): if one antenna “sees” an anti-node, the other will “see” a node. On the other hand, if the antennas are placed  $180^\circ$  apart, there is significant transmission. But, because the extra antenna would add more thermal mass into the system, it is recommended to make only reflection measurements.

During conditioning, the VNA will be physically disconnected and the positive terminal of the HV generator will be connected to the anode and the cathode will be grounded. Because the antenna is in contact with the anode, it will also be at the anode potential. The distance between the antenna and the surface of the anode ( $\text{delta\_antenna}$  in Fig. 5(b)) will be chosen to be on the order of a few millimeters to avoid electrical discharges between the antenna and the cathode. Every few pulse cycles or after a breakdown, the HV generator will be disconnected and the VNA will be connected to the antenna in order to measure the quality factor.

### Second design

Like in the previous design, a circular groove is machined into the surface of the anode, with a depth approximately equal to a quarter of the wavelength of the resonant mode. An antenna is now introduced through a hole made in the middle of the anode. Because of the central placement of the antenna, the  $TM_{110}$  mode, used previously, cannot be excited with this design. Instead, a higher order mode,  $TM_{010}$ , with axial symmetry, is used. The thickness and the inner radius of the choke will be the same as in the previous design, 2.7 mm, respectively 22.65 mm. Using eq. 7, we obtain a frequency of 7.6 GHz. Because of the higher frequency, the groove will be shallower in this design, making it easier to manufacture.

Unlike the previous design, the antenna cannot excite modes in the area between the choke and the edge of the electrode, making the notches superfluous and the design simpler. Unfortunately, if the antenna is recessed below the surface of the anode, the coupling will be very weak. But if the antenna is too close to the cathode, there is a risk of breakdowns between the cathode and the tip of the antenna. To fix this, a circular recession is drilled in the center of the cathode, with a diameter of 6 mm and a depth of 7 mm. A shallower recession, with a depth of 1 mm, but with a larger diameter (8 mm), is drilled in the anode to avoid the field enhancement effects on the

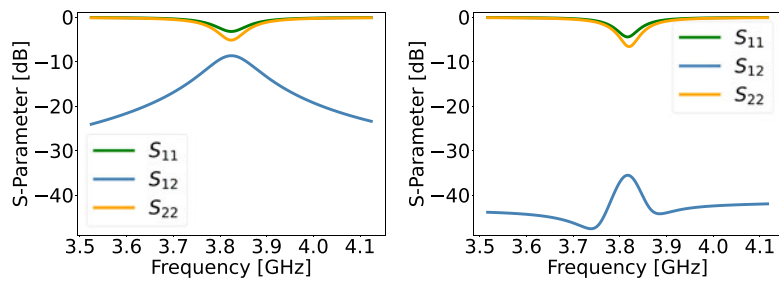


**Figure 6.** Simulated S-parameters in transmission configuration for antennas placed  $180^\circ$  (left) and  $90^\circ$  apart (right).

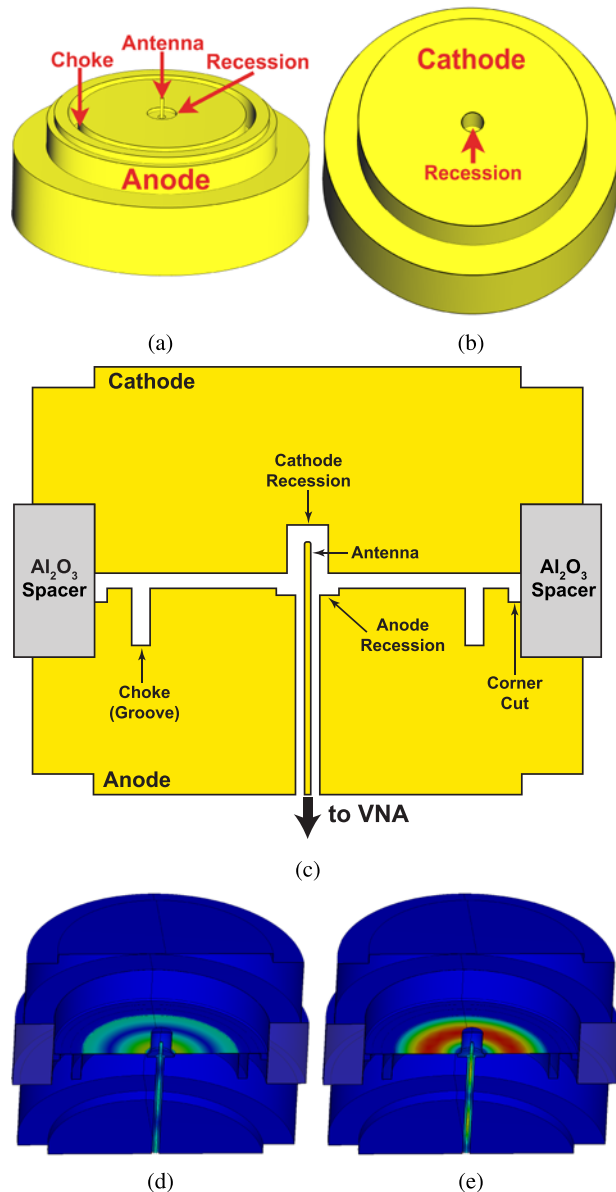


**Figure 7.** 3D model of the anode (a) and of the cathode (b), schematic showing a vertical cross-section through the electrode system (not to scale!) (c) and the electric (d) and the magnetic (e) field distributions for the  $TM_{010}$  resonant mode

edges of the cathode recession. To avoid field enhancement effects on the outer edges of the electrodes, a 2 mm deep cut is made in the edge of the anode, starting from 2 mm away from the edge. All these features are shown in Fig. 7(a)–(c).

The frequency of this design, with the added recessions, cannot be calculated using the analytical formula. Simulations in CST Studio Suite [36] show that the mode  $TM_{010}$  of this cavity has a frequency equal to 8.8 GHz. Therefore, the depth of the choke should be 8.5 mm. The quality factor at room temperatures obtained from simulations is  $Q_0 = 880$ , for a  $60 \mu\text{m}$  gap at 4K (and  $Q_0 = 58$  for a  $40 \mu\text{m}$  gap at room temperature).

The electric and the magnetic field distributions for this mode are shown in Fig. 7(d) and (e). The magnetic field has a field maximum in the shape of a ring with a radius equal to 12 mm and a thickness of approximately 8 mm, defining an area with the highest sensitivity to changes in resistivity.

During conditioning, the VNA is physically disconnected and the positive terminal of the HV generator is connected to the anode, while the cathode is grounded. The antenna will also be connected to the positive terminal to avoid electrical discharges between the antenna and the walls of the hole made in the anode. Every few cycles of pulses or after a BD, the HV generator will be disconnected and instead a VNA will be connected to the antenna, with the anode and cathode being grounded and the Q factor of the system will be measured.

## Experimental results

This first proposed design has been tested on a prototype manufactured in the Uppsala University's workshop, shown in 8(a). This design was tested at room temperature to check whether it works as expected. The gap size in these tests was  $75 \mu\text{m}$ . Using a vector network analyzer, the complex reflection coefficients were measured near the resonant frequency of the system, 3.7 GHz. These reflection coefficients, when plotted on a Smith chart, form a circle, as can be seen in Fig. 8(b). The Q-circle was fitted using the QFIT7 algorithm to obtain the quality factor and the coupling coefficient. Multiple such measurements were made, for different distances between the antenna and the anode surface, labeled  $\delta_{\text{anta\_antenna}}$  in Fig. 5(b). The measured quality factor at room temperature was 75, very close in value to the quality factor obtained from simulations. The coupling factor varies between 0.2 and 0.6, depending on the position of the antenna, as it is shown in Fig. 8(c).

A way to test whether we have coupled to the correct mode and not to the parasitic resonance is to make transmission measurements, using two antennas, placed either  $90^\circ$  or  $180^\circ$  apart. The fundamental mode we are interested in,  $TM_{110}$ , has electric and magnetic fields that vary along the azimuthal direction, such that an antinode is  $90^\circ$  away from a node and  $180^\circ$  apart from the next antinode. Therefore, it is expected to have little transmitted signal when the antennas are placed  $90^\circ$  apart, while at  $180^\circ$ , we expect significant transmission. As it is shown in Fig. 8(d) and 8(e), this exactly what we see: when the antennas are placed  $180^\circ$  apart,

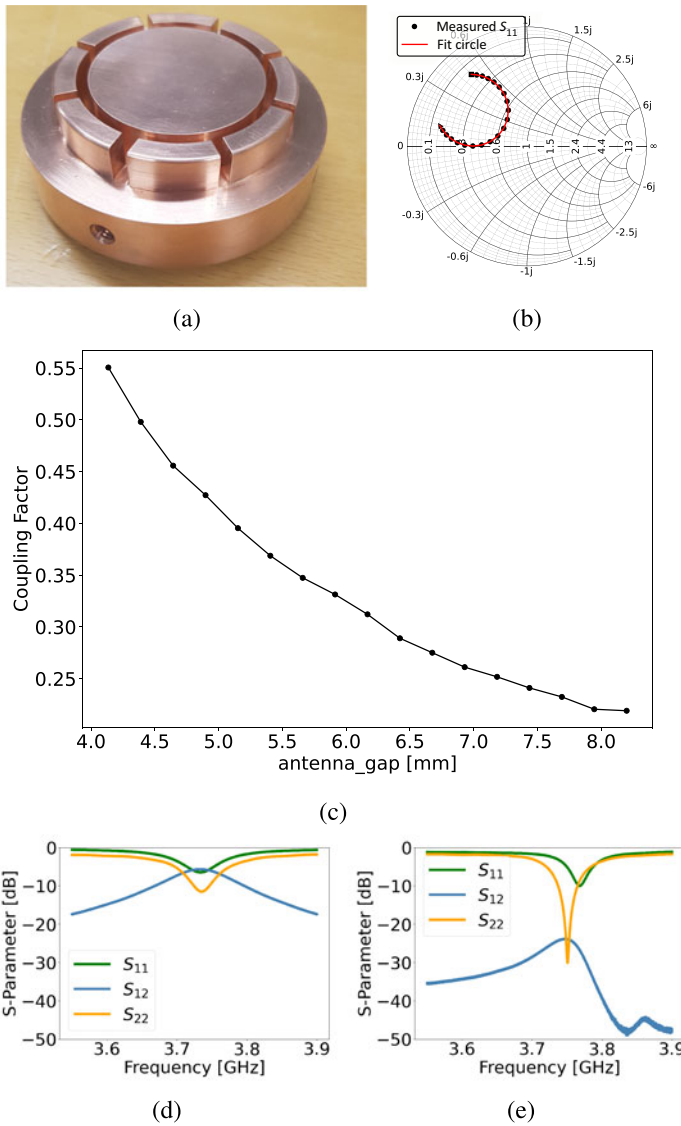


**Figure 8.** The prototype of the modified electrode for the first design (a), reflection coefficients, measured in the reflection configuration and fitted using the QFIT7 algorithm (b), the measured coupling factor as a function of the vertical distance between the tip of the antenna and the surface of the anode, labeled as *antenna\_gap* in Figure 5(b) and (c), the S-parameters in transmission configuration (antennas are placed 180° (d), respectively 90° apart (e)).

we have significant transmitted signal, while when the antennas are placed at 90°, the transmitted signal decreases by 17 dB.

On the other hand, the parasitic mode has its antinodes placed 90° apart. If we would have coupled to this mode, we would have measured significant transmission both at 90° and at 180°.

**Discussions and conclusions**

Understanding the causes of vacuum arc breakdowns is important for many areas of research and for many technological applications. Some experimental evidence suggests that one of the most important causes of the formation of vacuum arc breakdowns is the creation and movement of dislocations a few microns underneath the metal surface on which the field is applied.

While some studies managed to characterize conditioned surfaces exposed to high field looking for proof of this mechanism on and below the surface, the results are not conclusive. What is lacking is the direct evidence of changes *during* the conditioning process. This is what the method proposed in this paper will mitigate. We propose to make surface resistivity measurements during

HV conditioning. We plan to make measurements in cryogenic conditions to clearly measure the resistivity changes due to the movement and creation of crystallographic defects, using a resonant mode induced between parallel plate electrodes exposed to DC pulses. In order to be able to do this, the current design of the electrodes needs to be modified in order to act as a resonant system.

Two electrode designs have been studied, both featuring a circular groove machined in the anode, thanks to which the electromagnetic modes can be excited in the area circumscribed by the groove. The first design is advantageous because only one electrode needs to be modified, and enables measurements in both transmission and reflection configuration. The identified shortcoming of this design is the need to maintain good electrical contact between the antenna and some parts of the electrode when cooling down. This design was tested at room temperature, and the measured quality factor was found matching closely the value obtained from simulations, as it is shown in Table 1. The design was also tested in transmission configuration, confirming that the right mode was excited, while the parasitic mode was removed. The second design requires modification of both electrodes but guarantees a reliable

**Table 1.** Summary of the results for both designs

Design	Gap [ $\mu\text{m}$ ]	Temperature	$Q_0$
1 (Simulated)	40	RT	39
1 (Simulated)	60	4K	580
1 (Simulated)	75	RT	74
1 (Measured)	75	RT	75
2 (Simulated)	40	RT	58
2 (Simulated)	60	4K	880

electrical connection with a simpler arrangement. The results from simulations for both designs, at room temperature (RT) and in cryogenic conditions, at 4K, as well as the measured value of the quality factor of the first design at room temperature are shown in Table 1.

It should be mentioned that the presence of an RF antenna inside the system during conditioning opens the possibility for unique vacuum discharge diagnostics not used before, though it will require careful analysis to interpret the results.

This method of characterizing the resistivity of metal surfaces placed under high electrical DC fields might have further applications in other areas of research, for example, as a complementary technique in the characterization of thin films placed under high electrical fields [37] or superconducting novel materials [38].

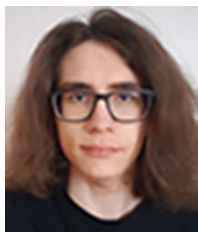
**Competing interests.** None declared.

## References

- Boxman RL, Sanders DM and Martin PJ (1995) Fundamentals and applications. *Handbook of Vacuum Arc Science and Technology*. New York: Noyes Publications.
- Burrows PN, Catalán Lasheras N, Linssen L, Petrič M, Robson A, Schulte D, Sicking E and Stapnes S (2018) The Compact Linear e+e- Collider (CLIC): 2018 Summary Report. CERN Yellow Reports: Monographs. 2(1), 23–35.
- Descoedres A, Levens Y, Calatroni S, Taborelli M and Wuensch W (2009) Investigation of the DC vacuum breakdown mechanism. *Physical Review Special Topics – Accelerators and Beams* 12(9), 092001.
- Saessalo A (2021) Experimental study of the role of extrinsic and intrinsic vacuum arc breakdown mechanisms. Ph.D. thesis, Helsinki U.
- Kojima H, Takahashi T, Hayakawa N, Hasegawa K and Sakaki M (2017) Optimum breakdown charge for maximum dielectric strength in spark conditioning in vacuum under a non-uniform electric field. *IEEE Transactions on Dielectrics and Electrical Insulation* 24(4), 2660–2665.
- Zhou Z, Kyrtsakis A, Wang Z, Li Y, Geng Y and Djurabekova F (2020) Effect of the anode material on the evolution of the vacuum breakdown process. *Journal of Physics D: Applied Physics* 54(3), 035201.
- Lachmann S, Jacewicz M, Profatlova I, Paszkiewicz J, Wuensch W and Ashkenazy Y (2021) Statistical analysis of field-emission currents. *Physical Review Applied* 16(2), 024007.
- Descoedres A, Ramsvik T, Calatroni S, Taborelli M and Wuensch W (2009) DC breakdown conditioning and breakdown rate of metals and metallic alloys under ultrahigh vacuum. *Physical Review Special Topics – Accelerators and Beams* 12(1), 032001.
- Degiovanni A, Wuensch W and Giner Navarro J (2016) Comparison of the conditioning of high gradient accelerating structures. *Physical Review Accelerators and Beams* 19(3), 032001.
- Descoedres A, Djurabekova F and Nordlund K (2009) DC breakdown experiments with cobalt electrodes. Tech. Rep., Geneva: CERN.
- Bagchi S and Perez D (2022) Atomistic modeling of the coupling between electric field and bulk plastic deformation in fcc metals. *Physical Review Accelerators and Beams* 25(3), 033101.
- Wang G, Simakov EI and Perez D (2022) Ab initio investigation of elastic properties of dilute Cu alloys for high-gradient accelerating structures. *Journal of Applied Physics* 132(17), 175112.
- Pohjonen AS, Djurabekova F, Nordlund K, Kuronen A and Fitzgerald SP (2011) Dislocation nucleation from near surface void under static tensile stress in Cu. *Journal of Applied Physics* 110(2), 023509.
- Pang W-W, Zhang P, Zhang G-C, Xu A-G and Zhao X-G (2014) Dislocation creation and void nucleation in FCC ductile metals under tensile loading: a general microscopic picture. *Scientific Reports* 4(1), 6981.
- Nordlund K and Djurabekova F (2012) Defect model for the dependence of breakdown rate on external electric fields. *Physical Review Special Topics – Accelerators and Beams* 15(7), 071002.
- Zadin V, Veske M, Vigonski S, Jansson V, Muszinsky J, Parviainen S, Aabloo A and Djurabekova F (2018) Simulations of surface stress effects in nanoscale single crystals. *Modelling and Simulation in Materials Science and Engineering* 26(3), 035006.
- Engelberg EZ, Ashkenazy Y and Assaf M (2018) Stochastic model of breakdown nucleation under intense electric fields. *Physical Review Letters* 120(12), 124801.
- Ashkenazy Y, Yasha A, Cohen O and Popov I (2022) Observations of dislocations in soft Cu samples exposed to high fields. In *10th International Workshop on the Mechanisms of Vacuum Arcs (MeVArC2023)*. Chania, Crete.
- Ashkenazy Y and Popov I, (2023) In-person miniMeVArC at CERN, 2023. *Characterizing electrodes – on Zebras and red Herrings*, Geneva, Switzerland.
- Engelberg EZ, Paszkiewicz J, Peacock R, Lachmann S, Ashkenazy Y and Wuensch W (2020) Dark current spikes as an indicator of mobile dislocation dynamics under intense DC electric fields. *Physical Review Accelerators and Beams* 23(12), 123501.
- Paszkiewicz J (2020) Studies of breakdown and pre-breakdown phenomena in high-gradient accelerating structures. Ph.D. thesis, Oxford U, Ph.D. thesis.
- Fonteyn D and Pitsi G (1987) SDR of copper plastically deformed by torsion at 4.2 K. *Solid State Communications* 64(8), 1113–1116.
- Ekin J (2006) *Experimental Techniques for Low-Temperature Measurements: Cryostat Design, Material Properties and Superconductor Critical-Current Testing*. Oxford: Oxford University Press.
- Brown RA (1982) The interaction of conduction electrons with dislocations and grain boundaries in metals. *Canadian Journal of Physics* 60(5), 766–778.
- Pozar DM (2012) *Microwave Engineering*. Hoboken: Wiley.
- Bass J, Hellwege K-H and Olsen JL (1983) Electrical resistivity, Kondo and Spin fluctuation systems, Spin glasses and thermopower. In *Landolt-Börnstein – Group III Condensed Matter 15a: Condensed Matter*, Springer-Verlag, Berlin Heidelberg.
- Reuter GEH and Sondheimer EH (1982) The theory of the anomalous skin effect in metals. *Canadian Journal of Physics* 60(1042), 336–364.
- Jacewicz M, Eriksson J, Ruber R, Calatroni S, Profatlova I and Wuensch W (2020) Temperature-dependent field emission and breakdown measurements using a pulsed high-voltage cryosystem. *Physical Review Applied* 14(6), 061002.
- Redondo LM, Kandratsyev A, Barnes MJ, Calatroni S and Wuensch W (2016) Solid-state Marx generator for the compact linear collider breakdown studies. In *2016 IEEE International Power Modulator and High Voltage Conference (IPMHVC)*, San Francisco, CA, USA, 187–192.
- Gregory A (2021) Q-factor measurement by using a Vector Network Analyser. NPL Report.
- Kajfez D (2003) Random and systematic uncertainties of reflection-type Q-factor measurement with network analyzer. *IEEE Transactions on Microwave Theory and Techniques* 51(6), 512–519.
- Coman M (2022) Feasibility study of resistivity measurement of metal surfaces to address potential dislocations caused by surface conditioning. Master's thesis FREIA: Uppsala University.
- Calatroni S (2020) A Mathematica Notebook for the calculation of the anomalous skin effect in copper. CERN Notes CERN-ACC-NOTE-2020-0029.



34. **Shintake T** (1992) The Choke Mode Cavity. *Japanese Journal of Applied Physics* 31(11A), L1567.
35. **Anders E, Linner P and Gevorgian S** (2001) Mode chart of electrically thin parallel-plate circular resonators. In *Microwaves, Antennas and Propagation, IEE Proceedings*, Vol. 148. New York, 51–55.
36. CST Studio Suite 3D EM Simulation and Analysis Software. <https://www.3ds.com/products-services/simulia/products/cst-studio-suite/>.
37. **Accettura C, David A, Sergey A, Adrienn B, Bertarelli A, Biancacci N, Calatroni S, Carra F, Caspers F, Valdivieso G-T, Guardia-Valenzuela J, Kurtulus A, Mereghetti A, Métral E, Stefano R, Benoit S, Mauro T and Vollenberg W** (2020) Resistivity characterization of molybdenum-coated graphite-based substrates for high-luminosity LHC collimators. *Coatings* 10(4), 361.
38. **Kleindienst R** (2017) Radio frequency characterization of superconductors for particle accelerators. Ph.D. thesis.



**M. Coman** received his M.Sc. degree in physics at Uppsala University, Sweden in 2022. He is now a PhD student working at the FREIA Laboratory for Research Instrumentation and Accelerator Development. His research interests include microwave measurement techniques, high gradient technology, DC and RF breakdowns in vacuum, electron field emission and cryogenic techniques.



**M. Jacewicz** obtained his M.Sc. degree in nuclear and medical electronics at the Warsaw University of Technology, Poland, in 1997 and the Doctor of Technology degree in High Energy Physics at Uppsala University, Sweden, in 2004. He worked as postdoctoral fellow at Uppsala University, Sweden, Forschungszentrum Jülich, Germany, and Laboratori Nazionali di Frascati, Italy, with several nuclear and particle physics experiments on

the development of solid and gaseous particle detectors. He is currently Assistant Professor at the Department of Physics and Astronomy of Uppsala University, working at the FREIA Laboratory for Research Instrumentation and Accelerator Development. His research interests include high gradient technology, DC and RF breakdowns in vacuum and electron field emission.



**D. Dancila**, in 2011, completed his Ph.D. in Microwave Engineering at the Université catholique de Louvain, focusing on research related to RF-MEMS and microfabrication technologies for millimeter-wave components, which was conducted at IMEC in Belgium. Since March 2019, he has held the position of Associate Professor at Uppsala University, where he currently teaches courses in electronics and microwave engineering. He is heading the microwave group and leads research activities within areas, such as millimeter-wave antenna arrays and reflect arrays, RF sensors, and high-power highly efficient RF and microwave amplifiers at the FREIA laboratory. In addition to his academic achievements, Dr Dancila possesses a formal education in Business Management, which he acquired from the Solvay Business School in Brussels. He has also founded the spin-off company Percy Roc AB, with a primary focus on material processing utilizing high-power microwave technology.